Full length article

Analysis of stresses and shape changes in thin substrates with stressed film patterning using femtosecond laser micromachining

Heng E. Zuo *, Ralf K. Heilmann, Mark L. Schattenburg

Massachusetts Institute of Technology, 77 Massachusetts Ave, Cambridge, 02139, MA, USA
Space Nanotechnology Laboratory, MIT Kavli Institute for Astrophysics and Space Research, 70 Vassar St, Cambridge, 02139, MA, USA

ARTICLE INFO

ABSTRACT

The accurate, high-throughput fabrication of light weight optical systems for applications like next-generation space telescopes and semiconductor wafers is both crucial and challenging. A potential solution is to first fabricate thin substrates with traditional methods, then apply surface stress to bend them into desired shapes to correct residual height errors. We have developed a stress-based figure correction method for thin silicon mirrors using a femtosecond laser micromachining technique to generate patterned stress fields, through the removal of selective stressed film regions and adjacent substrate regions. In this paper, we present an in-depth analysis for the laser-induced stresses and resulting shape changes of thin mirrors due to the periodic patterning of a stressed film (silicon oxide) on silicon substrates using femtosecond laser surface ablation. Experimental results are presented, and a 3D finite element model (FEM) is developed to study the substrate curvature in directions parallel and perpendicular to the patterned troughs in the substrates. We simulate the stress relief process in the thin-film/substrate system, and the numerical predictions compare reasonably well with curvature measurements for several different geometrical combinations of depth, width and spacing of the patterned troughs, achieving > 82% quantitative agreement with the experiments. It is also shown in the simulations that certain geometries of patterned troughs induce more dramatic shape changes and counter-intuitive reversals of curvature in the direction perpendicular to the troughs, and a qualitative explanation involving the Poisson effect is presented. The 3D finite element methods and findings of this paper can be used to determine the optimal parameters of the stressed film patterns for figure correction of thin telescope mirrors and other types of thin substrates used in the semiconductor industry.

1. Introduction

The growing interest, increasing demand and more stringent requirements for future lightweight, high-precision optical systems, such as space telescopes [1–3], wafer-flattening processes during semiconductor manufacturing [4–6], and other types of freeform optics for imaging [7], pose major challenges to the optic quality of the thin mirrors and substrates that are essential in these optical systems. For many ultra-lightweight space optics applications, traditional optical fabrication methods such as polishing, ion beam figuring and magnetorheological finishing fall short of meeting the exact shape requirements. For example, thin silicon optics are considered great candidates for a variety of space missions and are actively being researched for a number of space telescopes, from segmented mirrors for the next generation of space X-ray telescopes [2] to ultra-lightweight deformable mirrors [1]. However, it is very challenging to manufacture thin mirrors to exact shapes with high optical quality, because they tend to deform

easily during fabrication. In addition, the deposition of coatings that are used to enhance mirror reflectivity can distort thin mirror substrates beyond their acceptable tolerances. Therefore, it is critical to introduce a surface correction step to the mirror fabrication process to achieve high quality thin mirrors.

One such approach is the stress-based figure correction method, in which a 2D stress field is applied to induce controlled deformation and bend the thin mirror into desired shapes. The surface stress can be applied at or close to the back surfaces of mirror substrates to correct for shape errors and compensate for coating distortions without introducing additional surface height errors. Various approaches have been developed for this purpose, including piezoelectric film adjusting [8,9], ion implantation [10,11], and oxide patterning with photolithography and acid etching [12,13]. Many of these methods require numerous complex steps, stringent working environment (or large expensive machines), and/or consuming processing time, all of which make them to

---

some degree impractical to be applied to a large number of thin mirror shells that will be needed for many space telescope missions. Further, some of these attempts are focused on applying equibiaxial stress only, which is just one of the three planar stress components that can be used to represent a planar stress field (the other two are antibiaxial and shear components). This limits the types of mirror distortion that can be accurately corrected, but general stress fields are needed to achieve exact figure corrections [14].

Building upon aforementioned methods while avoiding some of their problems, we have investigated another approach, namely femtosecond laser micromachining, which combines advanced laser machining technology with the stressed film patterning method [15,16]. A layer of intrinsically stressed material is first deposited onto the substrate back surface, which then gets selectively removed with femtosecond lasers. By removing part of the stressed film and adjacent substrate regions in different areas across the surface, a certain fraction of the applied stress is relieved in a controlled pattern, resulting in a stress field that can reshape the thin mirror substrate and bend it into the desired shape. By incorporating the advanced ultrafast laser micromachining technique it surpassed many challenges of existing methods (such as secondary distortion and spring-back problems). As a fast and straightforward approach, it is intended to correct mirror figure error and achieve good accuracy, similar to oxide patterning with photolithography, but in a much simpler and cost-effective fashion for even high-level, complex systems.

A similar approach for fused silica optics using ultrafast laser micromachining has also been studied by various groups [15,17,18], where small stressed regions are created inside micron-scale focal volumes of ultrafast laser beams to induce stable deformation of glass plates. Both approaches in silicon and glass optics are applicable for correcting figure errors either before or after other structures and/or coatings have been applied to the optical surface.

A key component in this technique is to be able to generate all three stress components with stressed film patterning. It can be shown that this is equivalent to generate two types of planar stress components, i.e., equibiaxial and non-equibiaxial stress, while applying a proper rotation of the latter [14]. Therefore, the objective of this paper is to characterize the induced stresses and shape changes of thin mirror substrates processed with a stressed film patterning method using the ultrafast laser micromachining technique. We carried out a combined experimental and numerical investigation on thin silicon mirrors to answer the following question: what are the relationships between the induced stress fields and geometrical combinations of the depth, width and spacing of the applied pattern? To simplify the problem, we limit our experiments and simulations to thin, nearly flat mirror plates, but the results can be generalized to curved mirrors that are of interest to various telescope applications.

In this paper, we first review the experimental design and results for the model system of a silicon wafer with a stressed film of thermally grown silicon oxide (SiO_2) in which patterns of features have been ablated from the blanket film. Research has proved the growth of thermal oxides on silicon to be repeatable and stable, and it has an intrinsic compressive stress of in the range of $300\,\text{MPa}$ to $450\,\text{MPa}$, depending on a number of factors such as the growth temperature and substrate orientation [19,20]. Then, we explain why the simple analytical model of Kirchhoff–Love thin-plate theory cannot fully explain the observed results. Furthermore, a three-dimensional finite element model (FEM) is built using Abaqus for simulating substrate curvatures and stresses with different laser micromachined features in the stressed film patterns. Simulated substrate curvatures and stresses from two different types of micromachined features are shown and compared with the experimental results to demonstrate the effectiveness of the proposed methods. It is also shown that certain geometries of patterned troughs can induce a reversal of curvature in a certain direction in the thin-film/substrate system. The results are discussed in further detail.
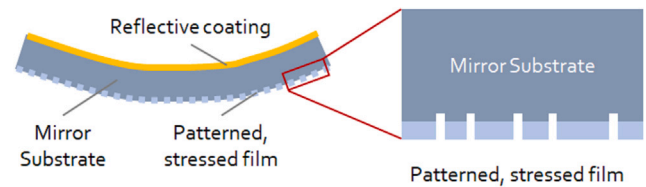

Fig. 1. Illustration of the stressed film figuring method for correcting thin mirrors with patterned stress fields, through the selective removal of stressed film regions and attached substrate regions.

2. Experiment and results

The mirror correction process includes several steps, starting with a bare silicon mirror with known figure errors. Detailed procedures and experimental setup are described elsewhere [16]. Here, we focus on understanding different residual stress fields and substrate curvatures from various pattern geometries. Since the stress effect of an individual laser ablated spot is almost negligible, we calibrate this effect by applying a uniform micromachining pattern across the entire substrate and measure the average change of curvature. Two patterns composed of periodic features — uniformly distributed holes and periodic troughs — are applied to the mirror substrate. We briefly review our procedure and summarize the results in this section.

Fig. 1 illustrates this method for correcting thin substrates with patterned stress fields, for which femtosecond laser micromachining is a promising candidate. The substrates are Si wafers of $100\,\text{mm}$ in diameter, $525(10)\,\mu\text{m}$ in thickness, and (100) surface orientation. A stressed film of thermal oxide is first grown on the back side of the silicon mirror, followed by deposition of highly reflective coatings on the front surface. The thickness of the oxide film should be chosen such that it can create enough bending moment to compensate for the original mirror distortion. In this experiment, we chose a number of different oxide thicknesses (ranging from $0.3\,\mu\text{m}$ to $1.4\,\mu\text{m}$) to help understand their influence. The surface profile of the mirror's front side is measured with an Apre interferometer before and after each step, and the change in the profile is used to reconstruct a surface height change map. This is then compared to the target shape to generate an error map that is to be corrected. A stress field that can correct for this error map can be calculated in a number of ways, such as shown by Chalifoux et al. [14]. Then, femtosecond laser pulses are focused on the thermal oxide film at the back surface to ablate a series of features such as holes or troughs, whose dimensions are on the order of $10\,\mu\text{m}$. The removal of the stressed film inside these features allows the materials in adjacent regions to relax, resulting in stress relaxation and substrate bending. To apply the pattern over the full mirror, the substrate is moved perpendicularly to the laser beam to expose various regions across the whole substrate.

The femtosecond laser micromachine system presented in this paper is an AOFemto™ series diode-pumped solid-state laser (Advanced Optowave Corporation, Ronkonkoma, NY), which delivers a femtosecond laser beam with pulse width of $\tau = 800\,\text{fs}$ and repetition rate of $100\,\text{kHz}$ at a green light wavelength of $\lambda = 515\,\text{nm}$. The waist of the Gaussian beam at the focus is about $9\,\mu\text{m}$ in diameter. A galvo scanner allows for very fast scanning speed – up to $3000\,\text{mm/s}$ in its field of view (30 mm × 30 mm). The mirror substrate is mounted on top of a motorized X–Y translation stage that moves perpendicular to the laser beam to enable the stitching of different fields to cover the whole substrate. With this setup, a $100\,\text{mm}$ wafer can be micromachined in a few minutes.

We have examined micromachined features with various micromachining parameters with this setup. Examples of two micromachined features taken with a confocal microscope are shown in Fig. 2. The sample under test has a $0.5\,\mu\text{m}$ thick thermal oxide layer on the test surface in both examples. In Fig. 2(a), the image of a micromachined
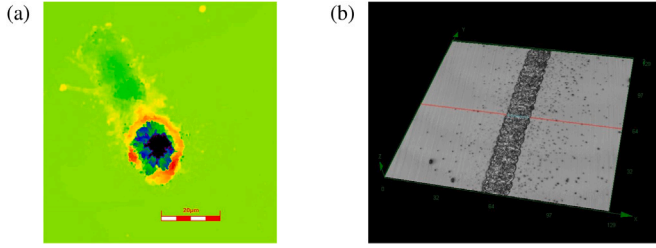
Fig. 2. Confocal microscope images of two micromachined features: (a) a micromachined hole exposed to 100 consecutive laser pulses; (b) a micromachined trough exposed to continuous laser pulses.

Fig. 3. Laser-induced integrated stress fields in eight silicon wafers with 500 nm–thick single-side thermal oxide, machined with periodic trough patterns. The trough period is 200 μm for all samples, but they have different trough geometries (width and depth) since they were machined with different parameters. The individual integrated stress components in two axial directions X and Y for each sample are marked by orange and blue squares, and their different magnitude shows that non-equibiaxial stress fields are generated in this series of tests. The horizontal and vertical error bars represent the uncertainty in trough measurements and stress calculations.

Table 1

Micromachining results in eight silicon wafers with 500 nm–thick single-side thermal oxide, machined with 200 μm periodic trough patterns.

Label	Trough depth /Trough width [%]	Integrated stress S_{xx} [N/m]	Integrated stress S_{yy} [N/m]
1	9.8 ± 0.7	44.7 ± 1.3	40.2 ± 1.7
2	13.0 ± 2.3	44.3 ± 2.8	37.4 ± 3.8
3	13.4 ± 2.2	50.6 ± 0.8	41.5 ± 0.7
4	19.9 ± 1.7	57.9 ± 1.6	42.8 ± 1.2
5	20.0 ± 2.6	57.5 ± 9.1	44.1 ± 8.5
6	40.8 ± 6.1	80.8 ± 4.2	49.2 ± 1.9
7	53.8	115.3 ± 17.0	53.6 ± 6.4
8	87.5	159.9 ± 20.5	76.1 ± 8.2

hole is shown, which is exposed to 100 consecutive laser pulses with pulse energy of 20 μJ. The micromachined hole diameter is 14 μm, with a depth of ≥15 μm. In Fig. 2(b), a micromachined trough is shown, which is exposed to continuous laser pulses of pulse energy 1 μJ and a scanning speed of 500 mm/s. The trough width is 15 μm with a depth of 0.25 μm after micromachining. Additional characterization figures such as SEM and LCM images and further experimental details can be found in Zuo et al. [15], Zuo [21] and Zuo et al. [16].

To characterize the change of the stress state across the substrate caused by the micromachining process, we first obtain the reconstructed surface height change map from the difference between before and after interferometer measurements by fitting to a set of Zernike polynomials. The curvatures can be obtained from the surface height change map, by numerically taking the second order derivatives of the displacement field. The deformation of the thin-film/substrate system is proportional to the stress in the film integrated over its thickness, or the mean film stress multiplied by its thickness, also known as the integrated stress. The relationship between the integrated film stress field (S_{xx}, S_{yy}, S_{xy}) and substrate curvature changes can be described by Stoney's equation [22,23]. In Cartesian coordinates, the relationships can be written as:

$$S_{xx} = \frac{E_s h_s^2}{6(1-\nu_s^2)}(\kappa_{xx} + \nu_s \kappa_{yy}),$$
$$S_{yy} = \frac{E_s h_s^2}{6(1-\nu_s^2)}(\nu_s \kappa_{xx} + \kappa_{yy}), \quad (1)$$
$$S_{xy} = \frac{E_s h_s^2}{6(1-\nu_s)}\kappa_{xy},$$

where E_s and ν_s are the Young's modulus and Poisson's ratio of the substrate, h_s and h_f are the thickness of the substrate and film, respectively, and they need to satisfy $h_f \ll h_s$ [23]. In addition, $\kappa_{xx}, \kappa_{yy}, \kappa_{xy}$ are the curvature changes of the thin-film/substrate system, where the former two are the curvature changes in X and Y directions, and the latter represents a twist of the substrate's midplane. The above formula can provide the stress map of the thin mirror (thin-film/substrate system) from measurements of its surface profiles. It is also worth mentioning that when applying the above equation in this work, the whole substrate surface including the surface patterns is considered as a continuous stressed film that averages over small features. This can be justified because the micromachined features (holes or troughs) in this work are small in size compared to the substrate thickness, and the length scales of the figure errors that need to be corrected are large compared to the individual feature size.

A large number of substrates has been processed using the aforementioned process with both uniformly distributed hole and periodic trough patterns. We have shown that uniformly distributed hole patterns create equibiaxial stress states, where the residual integrated stress fields in two orthogonal directions X and Y are very close to each other in magnitude [15]. In a recently submitted paper [16], we show that periodic troughs generate a non-equibiaxial stress state. Laser ablation of troughs in the stressed film creates different bending
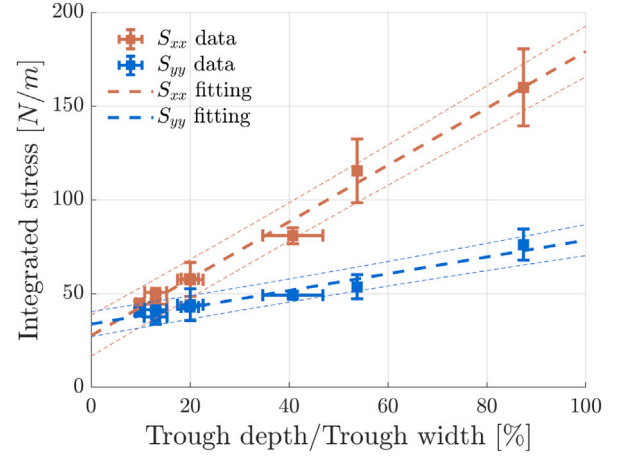
moments for the mirror substrates in the two directions perpendicular (X direction) and parallel (Y direction) to the troughs. Higher tensile stress field is measured in the X direction as more original compressive film stress is relieved in this direction.

We also found that at small trough depths (within a few μm), the laser induced stress relief effect forms a quasi-linear relationship with the ratio of trough depth divided by trough width. The dash lines in Fig. 3 represent linear fits (with 95 % confidence interval) to each set of data of the same color. This quasi-linear relationship, however, does not hold when the trough depth becomes large relative to its width. We will discuss this after the next section. It is also worth noting that there is a certain level of uncertainty in the measurements, which mainly comes from variations in trough geometry measurements and curvature measurements of the relatively small overall substrate deformation. The uncertainty in the measurements as well as in the stress calculations are represented by horizontal and vertical error bars for each data point. The same data is also shown in Table 1. The experiments showed that femtosecond laser ablation of stressed films can effectively change the surface figure of thin mirror substrates by introducing controlled bending.

In addition, we examined the micromachined samples using Raman spectroscopy, in the hope to find any structural or phase changes in the samples after micromachining. We did not, however, see a clear pattern of frequency shifts in those samples near the irradiation zone. Therefore, we could not conclude whether or not there were phase changes in those samples from the spectroscopy examination, though
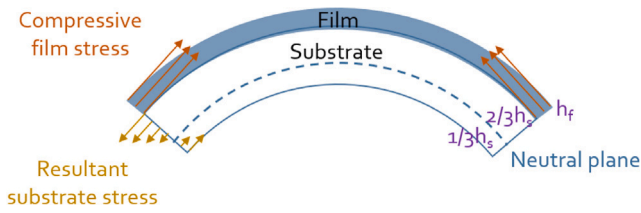
Fig. 4. Illustration of a deformed substrate under a uniform compressively stressed film. The red arrows in the film show the compressive film stress, while the yellow arrows in the substrate indicate that the substrate is curved due to the film stress. A neutral plane, neither compressed nor expanded, is illustrated in the substrate by a dash line and located at $2/3 h_s$ from the film–substrate interface.
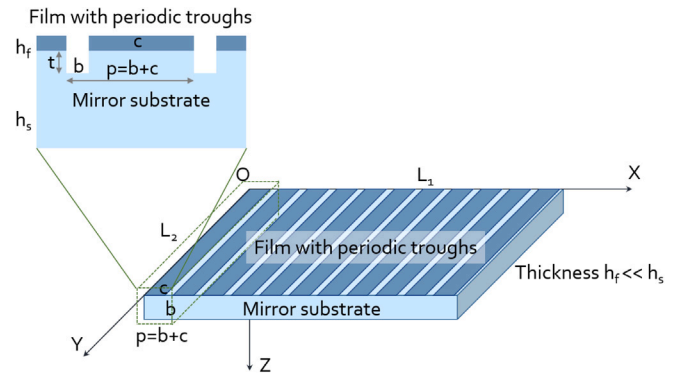

Fig. 5. Illustration of the thin-film/substrate system with periodic trough structures. The enlarged area to the top left illustrates a cross-section of the periodic trough structures. The side (Y–Z) planes of the periodic troughs are perpendicular to the film/substrate interface, and the trough is at least deeper than the film thickness, i.e., $t \geq 0$.

such phase changes in Si samples have been shown by Smith et al. [24] and Ionin et al. [25]. It is also worth noticing that due to the existence of the thermal oxide film on the surface of the Si substrates, the photonic energy is primarily deposited and absorbed by the film, while only a small portion of the deposited energy can reach the Si substrate beneath the film. We suspect phase changes in the Si substrates may occur during the micromachining and may contribute to the stress relief that we measure, but we believe the effect is predominantly due to the removal of stressed film. As a comparison, Yao et al. [13] have shown that photolithography and chemical (HF) etching can be used to created vertical features in Si substrates with thermal oxide films, and similar stress relief results have been observed in those experiments. The similarity in the results suggests that the stress relief effect we present in this paper is dominated by the removal of oxide patterns through ablation, while the contributions from other processes of stress changes in the samples must be small. Moreover, since our primary interest of this paper is in the application of femtosecond laser micromachining to create predictable changes to thin mirrors on a much larger scale, i.e., the stress and curvature changes of the whole substrates, we do not intend to focus on the micro-structural changes in the Si structures and/or post-ablative characterization. The mechanism for the stress relief effect from the removal of stressed films, and a complete analysis and comparison between experiments and numerical predictions for the patterning, are the subject of next section.

3. Numerical modeling

3.1. Limitations in theory and previous numerical models

The bending of a thin mirror substrate under a uniformly stressed film (also referred to as the "blanket film") can be solved analytically using the Kirchhoff–Love thin-plate theory, which is a two-dimensional mathematical model to determine the deformations and stresses in thin plates subjected to forces and moments. The theory assumes that a neutral plane can be used to represent a three-dimensional plate in two-dimensional form. To model a thin mirror substrate with a layer of stressed film, the original transverse load is replaced with an in-plane stress load applied by the film with intrinsic stress of $\sigma^{(f)}$. The film thickness h_f needs to be much smaller than the substrate thickness h_s, which is also at least 10 times smaller than its lateral dimensions. The neutral plane is not the mid-surface of the plate: it is assumed to be located inside the substrate at a depth of ah_s, $0 \leq a \leq 1$ from the film–substrate interface.

Two approaches can solve this problem: to balance the forces and moments at any cross-section in the thin-film/substrate system, or to minimize the total potential energy of the substrate. Formulations and detailed derivations can be found in Freund and Suresh [23] and Zuo [21]. For the special case of a thin mirror substrate bending under a uniform film, the solution becomes the Stoney's equations for equibiaxial film stress. The neutral plane is at $a = 2/3$ of the substrate thickness, and resulting substrate curvatures are $\kappa_{xx} = \kappa_{yy} = -\frac{6(1-\nu)\sigma^{(f)} h_f}{E h_s^2}$, $\kappa_{xy} = 0$.

The negative sign in the curvature indicates negative (compressive) membrane force. This result is illustrated in Fig. 4.

On the other hand, the bending of a substrate under nonuniform films is a much trickier problem, and neither force balance or energy approach can give accurate predictions of non-equibiaxial stress states. In the case of a periodic array of parallel troughs (period p) formed in the stressed film along the X axis (see Fig. 5), the above approach still gives an equibiaxial solution. The only difference is that both curvatures in two axial directions are scaled down by a factor of $\eta = \frac{c}{p}$, which is the area fraction of the residual film over the whole substrate [21]. This result credits the proportional decrease of the curvatures in the resultant thin-film/substrate system to purely the removal of the film area from laser ablation. It does not, however, capture the anisotropic, non-equibiaxial behavior of the measured laser-induced stresses and substrate curvature changes in the experiments with periodic trough patterns.

The primary reason for this discrepancy is that the formation of the troughs in the stressed film (and adjacent substrate) changes the local stress distribution near the troughs and creates an immediate stress relief effect, because the normal stress that acts on the side faces is reduced to zero. This leads to a decrease of film stress (also referred to as σ_m, the "mismatch stress"), and a decrease in the "artificial membrane force" that is needed to balance the new internal stress in the periodic film/substrate system. Without knowing the extent of this mismatch stress reduction, we would not be able to apply the proper force in the boundary value problem for the thin-film/substrate system with periodic troughs. Therefore, to estimate the curvature change of the substrate due to the formation of periodic troughs, it is necessary to determine the real value of the resultant force in the boundary value problem.

Freund and Suresh [23] point out that the change in the equivalent membrane force Δf due to trough formation in a uniform stressed film, can be determined directly by means of the finite element method. Indeed, the next half of this section is devoted to the finite element modeling analysis of this problem. Alternatively, it is possible to estimate the numerical value of Δf from known measurements. This estimation is, however, material and geometry specific. For example, when the elastic properties of the film and substrate are identical, this term [26] is approximately $\Delta f \rightarrow 1.258\pi\sigma_m h_f^2/p$ as $h_f/p \rightarrow 0$. This results in a change of substrate curvature of $\Delta\kappa/\kappa^* \rightarrow 1.258\pi h_f/p$ as $h_f/p \rightarrow 0$, where κ^* is the substrate curvature of a continuous blanket film. An approximation for all values of h_f/p in bimaterial systems has been given by Xia and Hutchinson [27], which renders $\Delta f \approx -\frac{l h_f \sigma_m}{p} \tanh(\frac{p}{l})$, $\Delta\kappa \approx -\kappa^* \frac{l}{p} \tanh(\frac{p}{l})$, where l is a parameter with physical dimension of length that is proportional to h_f, contingent on Dundur's parameters [28].

In short, it is not possible to obtain local stress distributions solely from analytical approaches for the problem where a nonuniform thin film is bonded to a substrate plate, so computational methods are still necessary to derive numerical solutions for mirrors with micromachined troughs. Though some approximation to the solution of this problem exists for a bimaterial system, the formulation is limited to a few materials and the approximation is only for one special case of the trough structure, where the troughs exist only in the film but not in the substrate, which is referred to as the "periodic film model" in the rest of this paper. (In comparison, the cases where troughs extend into the substrate are referred to as the "periodic film/substrate model".)

There have been some numerical studies for the deformation of layered structures composed of a series of parallel lines on a substrate. Previous work by Shen et al. [29] on the evolution of stresses and curvature changes due to the patterning of silicon oxide lines on silicon wafers studies a similar structure, but they also only consider one special scenario, where the trough depth is equal to the film thickness. We are, on the other hand, interested in a broader range of scenarios where the depth of the troughs can be much deeper than the film. Since the absorption process with ultrafast lasers is relatively material independent, which enables fabrication in compound substrates composed of different materials, more feature geometries can be micromachined in the thin-film/substrate system compared to traditional MEMS methods.

Some 2D FEM simulations [30] have been used to study the structure of interest, where the thin film is represented by shell elements. They only considered one cross-section of the problem perpendicular to the troughs, but this simplification virtually constrains the substrate displacement along the trough direction and sets its curvature changes to zero, i.e., $\Delta\kappa_{yy} \equiv 0$. This is not a proper assumption if we want to consider the bending along the trough direction. Therefore, a numerical model based on 3D FEM formulation would enable more accurate predictions for the stress and curvature changes in thin mirror substrates caused by various micromachined features, as it accounts for substrate deformation in directions both perpendicular and parallel to the troughs.

3.2. Formulation & model setup in Abaqus

The primary objective is to simulate the changes in substrate curvatures and stresses due to the formation of different laser micromachined features when applying the stressed film patterning method. Specifically, we map the changes of mirror curvatures and stresses as functions of feature geometries, including film period, and trough (or hole) depths and widths, through micromachining in a stressed thermal oxide film on silicon substrates. This correlation can be used to infer other micromachining parameters to create desirable features for its application in optics correction.

A three-dimensional finite element model is built using the FEM software Abaqus. The model simulates an internally stressed thermal oxide film bound to the surface of a flat silicon substrate, which is initially stress free. Since the model scale in lateral dimensions (in-plane of the plate) is much greater than its scale in the vertical dimension (along the thickness of the plate), fully capturing both scales requires very fine mesh size in a very large region. This would result in an exceedingly large number of elements and long program running time. To reduce the modeling difficulty and decrease the total number of elements in the model, without loss of generality, the model size is reduced to only 1/10 of the actual size, while still satisfying the thin-plate assumption, where the lateral dimension of the plate is at least 10X larger than its thickness. The reduced model can replace the full model in terms of predicting substrate curvatures, because the bending in a thin plate in theory does not depend on lateral sizes. It is the thicknesses of the film and substrate that matter. The model size can be reduced further by taking symmetry into account. Because a free-standing substrate is symmetric about its two mid-planes — XOZ plane and YOZ plane — only a quarter of the reduced size problem

needs to be modeled (see Fig. 5). For this reduced model, the lateral dimensions have been reduced to 5 mm. The substrate thickness is set to be 500 μm, and the thin-plate assumption still holds. In addition, fillets of 1.5 μm radius are used in the simulation to approximate the experimental results visible in SEM and LCM images. In addition to the two mirror symmetries for the YOZ and XOZ planes, the substrate is fixed in all 6 degrees of freedom (DOF) at the origin O. The substrate and film are joined together at the interface by a tie constraint, such that there is no relative motion between the two separate surfaces. The materials are chosen to replicate the real scenarios. The substrate material is a standard (100) silicon wafer that is orthotropic elastic. Its three axes are at [110], [1$\bar{1}$0], [001], and the Young's modulus (E), Poisson's ratio (v), and shear modulus (G) for this orientation are as follows: $E_x = E_y = 169\,\text{GPa}$, $E_z = 130\,\text{GPa}$, $v_{yz} = 0.36$, $v_{zx} = 0.28$, $v_{xy} = 0.064$, $G_{yz} = G_{zx} = 79.6\,\text{GPa}$, $G_{xy} = 50.9\,\text{GPa}$ [31]. The film material is an isotropic elastic thermal oxide (SiO$_2$), with approximate values $E = 70\,\text{GPa}$ and $v = 0.17$ [32].

Since the film/substrate system is free from external forces, there are no external loads applied to the system. Instead, a predefined field is applied to the film where its stress is directly specified to a known compressive value. The value of this predefined compressive stress is determined from the measurements of the film stress in the silicon wafers that were used in the experiments. The target is that when we input this predefined stress σ_0 as the initial condition for the film, the resultant film stress when the system reaches equilibrium is equal to the measured film stress $\sigma^{(f)}$ in the silicon wafers that are used in the experiments. It takes some trials to obtain the proper value for the magnitude of the predefined compressive stress, for which we performed a series of simulations with a uniform blanket film. The definition of this initial value for the predefined compressive stress field in the film is the initial condition of this problem.

To simulate a nonuniform film with periodic structures of either holes or troughs that are formed from laser ablation, these features are defined in the film/substrate system in the initial step before the analysis starts. The predefined stress field still is defined inside all of the film, even though it might be separated into non-connecting sections. As this predefined stress field is only applied to the film while the substrate is initially stress free, the difference between these two initial stress fields will create volumetric strains at the interface of the film and substrate. The analysis is completed when the film/substrate system reaches equilibrium, and the tie constraint enforces the film and the substrate to take on identical displacements at the interface. The result is a curved film/substrate system, where the resultant film stress is smaller than its initial value in the predefined field while the substrate develops an internal stress field to balance the film stress.

Two types of model and mesh have been used and compared: a fixed model with a structured hexahedral mesh, and an adaptive model with an unstructured tetrahedral mesh. The structured mesh of hexahedral elements has more inner nodes, and is generally more accurate. But the fixed model requires manual division of the structure into different parts for mesh generation, and has limited precision, depending mostly on the mesh size and quality. In order to create a finer hex mesh, extensive manual labor is required. The unstructured mesh of tetrahedral elements has fewer inner nodes, and is generally less accurate. But the adaptive remeshing process can adjust the mesh size to minimize the element energy density targets for the model. Therefore, high-quality results can be obtained with unstructured meshes, which can be created robustly and automatically with adaptive meshing algorithms. The fixed model can be used with both structured and unstructured meshes, but it does not have any advantage over an adaptive model if using the unstructured mesh. On the other hand, the adaptive model can only work with an unstructured mesh. Having tested both types of models, we chose the adaptive model with unstructured tetrahedral mesh as the main method, because the adaptive remeshing process can iteratively generate multiple dissimilar meshes to obtain the optimized mesh that satisfies the mesh discretization error indicator targets, while
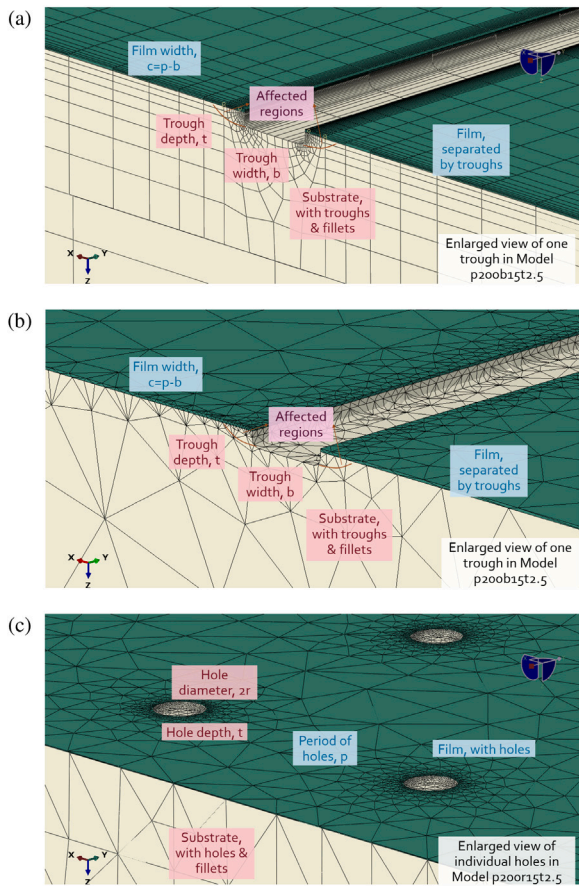
Fig. 6. Enlarged view of three models with a combination of two pattern structures and two types of meshes: (a) Periodic trough pattern with structured hexahedral mesh; (b) Periodic trough pattern with unstructured tetrahedral mesh; (c) Periodic hole pattern with unstructured tetrahedral mesh. The trough width and hole radius are both $15\,\mu m$.

minimizing the number of elements and, hence, the cost of the analysis. Fig. 6 shows three models with a combination of two structures and two types of meshes. Note that it is not possible to discretize the model with hole pattern using the structured mesh, due to its irregular configuration.

We first validated the model with the uniform blanket film since its analytical solution is known. The displacement plot shows that the substrate deformation is dominated by the transverse displacement (or, out-of-plane displacement), which agrees with the Kirchoff–Love thin-plate theory. Since the stressed film is isotropic in this case, the simulated curvatures have the same value in the two axial directions. The average residual film stresses obtained by just taking the average of the resultant film stress for every element in the film section of the model is an equibiaxial stress of $\sigma^{(f)} = 420\,MPa$, which matches the measured stress of the thermal oxide films used in the experiments.[1] Further, the resultant stress field in the substrate is equibiaxial as the stresses in the two axial directions are the same, and they match with the analytic solution $\sigma_{xx}^{(s)} = \sigma_{yy}^{(s)} = -\frac{6h_f\sigma^{(f)}}{h_s^2}\left(z - \frac{2}{3}h_s\right)$. It is also seen that the neutral plane in the substrate is indeed at 2/3 of the substrate thickness, in agreement with the theory.

Next, both periodic hole and trough pattern structures are modeled. One example of the geometries used in the trough model is as follows: period $p = 200\,\mu m$, trough width $b = 15\,\mu m$, trough separation (or film width) $c = p - b = 185\,\mu m$, trough depth (referring to the depth into the substrate) $t = 2.5\,\mu m$, and film thickness $h_f = 0.5\,\mu m$. The results for these simulations are shown in the next section.

3.3. Results

The question addressed here is the following: When the nonuniformity in the stressed film varies periodically along the interface, either in one direction or in two orthogonal directions, what changes in the resultant substrate curvatures can be created, and what factors contribute to the changes? First, we take a qualitative look at the two types of models with the same feature dimensions. Fig. 7 shows the simulated resultant stresses (von Mises) in the cross-section of the thin-film/substrate system for both models with periodic holes and periodic troughs, shown to the same scale. In both cases, the depth of the feature is $t = 15\,\mu m$, and the hole diameter is the same as the trough width, which is also $t = 15\,\mu m$. We find a significant resultant substrate stress, concentrated near the film/substrate interface along the wall (regions highlighted with red squares) of the ablated features (holes and troughs). The resultant substrate stress in these regions is tensile, which balances part of the compressive film stress in the thermal oxide. It is this edge effect that contributes to the additional stress relief when machining into the mirror substrate; whereas in the case that the feature only exists in the film, the stress relief can only come from the decrease of the compressive film stress at the edge of the film. Therefore, machining within the substrate enables more effective stress relief.

The figures clearly depict the bending moments towards the inside of the features from the film and substrate at the edge of the holes. This direction of the bending moments is also caused by the intrinsic compressive stress in the film, because the substrate at the interface with the film will try to expand to counteract this compressive film stress. If the intrinsic film stress is tensile, the bending moments would pull the edges away from the holes. In addition, the resultant stress field in the hole pattern model is much higher than in the trough model, which means its stress relief effect is not significant, due to less removed film material and less significant edge effects.

3.3.1. Simulated stresses & curvatures in uniformly distributed hole patterns

Several series of simulations were performed with periodic hole patterns. One model series is denoted as "p200r15", indicating that the period between the holes in both axial directions is the same, $p = 200\,\mu m$, and the radius of the holes is $r = 15\,\mu m$. The depths of the holes t in the models vary from $0\,\mu m$ to $22.5\,\mu m$, simulating the effect from different laser micromachining parameters. Note that in this work, the depth of the feature only refers to the depth that feature extends into the substrate, not counting the film thickness. By default, the feature is at least as deep as the film. This is the main difference between the models developed in this work ("periodic film/substrate model") and the ones studied by other authors, who primarily consider features in the film alone ("periodic film model").

The resultant curvatures and stresses from all hole depths are summarized and plotted in Fig. 8. Simulated resultant substrate curvatures normalized by κ^* for the series of models with uniformly distributed hole patterns (p200r15) are shown in Fig. 8(a). κ^* is substrate curvature in a uniform blanket film given by $\kappa^* = -\frac{6(1-\nu)\sigma^{(f)}h_f}{Eh_s^2}$, which is also the same as the substrate curvature before micromachined holes are introduced into the substrate. At $t = 0$, the substrate curvature is less than κ^* by $\sim 1.6\,\%$ purely due to the removal of the oxide films. This can be compared with the film removal percentage, which is $\pi r^2/p^2 \approx 1.77\,\%$. Both curvatures have essentially the same magnitude, because the holes are equally spaced into the two axial directions X and Y. The curvatures decrease gradually with increasing hole depth,
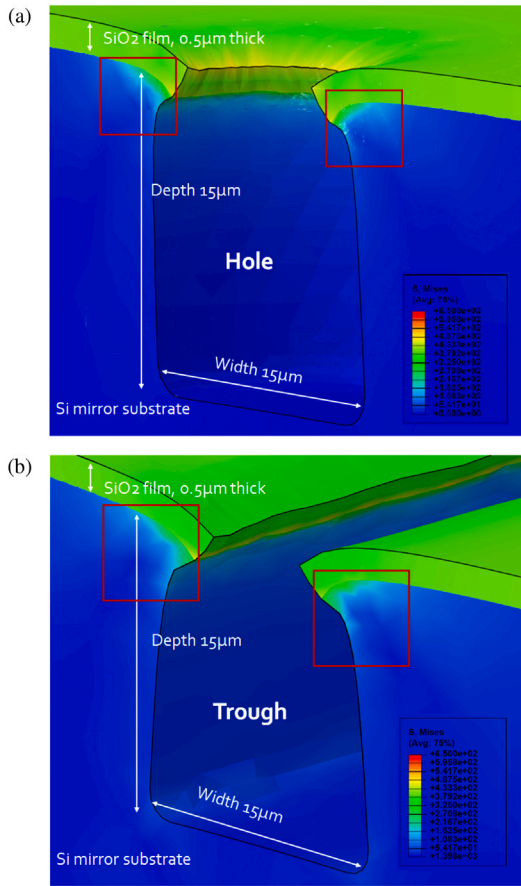
Fig. 7. Simulated resultant stresses (von Mises) in the cross-section of the thin-film/substrate system for both models with periodic holes (a) and periodic troughs (b), shown to the same scale (maximum 650 MPa).

Fig. 8. Simulation results from the series of models with uniformly distributed hole patterns (p200r15): (a) Simulated resultant substrate curvatures normalized by κ^* (substrate curvature in a uniform blanket film, given by $\kappa^* = -\frac{6(1-\nu)\sigma^{(f)}h_f}{Eh_s^2}$); (b) Simulated resultant average film stresses normalized by $\sigma^{(f)}$ (intrinsic compressive stress of a uniform blanket film, also the same as the film stress before micromachining).

and asymptotically approach a constant value (which is 96.7 %κ^* in this specific case). This asymptotic value of the curvatures, however, is not a constant number. Instead, it depends on two other dimensionless parameters r/p and h_f/r.

We can also plot the simulated resultant average film stresses normalized by $\sigma^{(f)}$ from the (p200r15) series in Fig. 8(b). $\sigma^{(f)}$ is the intrinsic compressive stress of a uniform blanket film, also the same as the film stress before micromachined holes are introduced into the substrate. The normalized percentages of the resultant average film stress are actually the same as the percentages of the normalized curvature, which is essentially because the resultant stress field is equibiaxial in this model. Using Stoney's equations, we can easily show that in an equibiaxial system the integrated stress field scales linearly with curvature. The curves also indicate that increasing the hole depth into the substrate for a given hole radius will lead to larger stress relief, but this increase does not last for long. When the hole depth increases to about 50 % of its diameter, the normalized average film stress will stop changing with even deeper holes.

3.3.2. Simulated stresses & curvatures in periodic trough patterns

Several series of simulations are performed with a periodic trough pattern. The three most studied series are "p200b15", "p100b15" and "p50b15", where p is the period of the parallel trough structures, and b is the width of the trough. Some authors prefer looking at the width of the film strips rather than the trough widths (also called the trough separation in this paper, as $c = p - b$). Similar to the pattern with uniformly distributed holes, the depth of the troughs is at least as deep as the film thickness and t starts from zero at the interface of the film
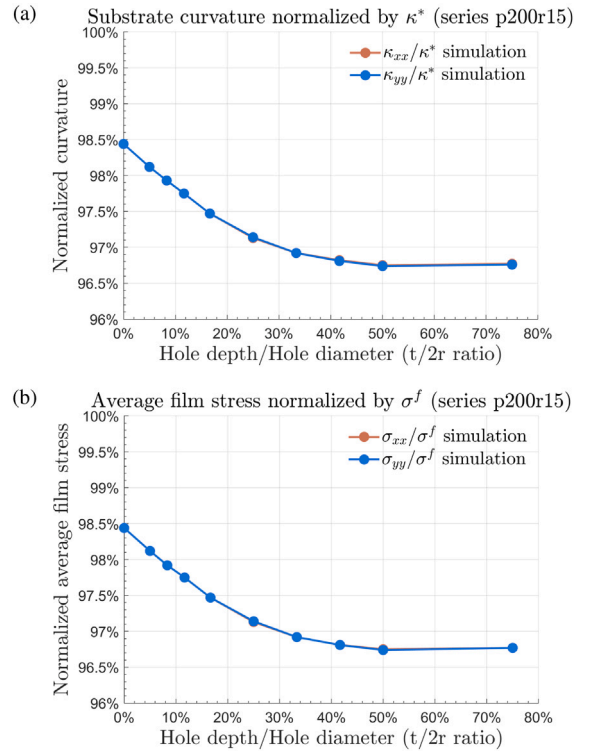
and substrate. Varying p and t together allows us to simulate the effect from more laser micromachining parameters.

Similar to the model with periodic holes, a considerable amount of bending moment forces the substrate and film materials along the trough walls to bend inwards. A "small piece of substrate material", or more precisely, a differential element in the substrate at the interface will try to expand to counterbalance the compressive stress imposed by the film. But the motion along the direction of the trough is confined by other differential elements like itself, so it cannot move in that direction. As a result, it expands much more prominently in the direction perpendicular to the trough, and hence, relieving much more of the originally isotropic film stress in the direction where it expands.

The above mechanism results in a non-equibiaxial substrate stress, concentrated near the film/substrate interface along the wall of the ablated troughs. The resultant substrate stress near the interface is tensile, to balance part of the compressive film stress in the thermal oxide. The magnitude of this stress is also larger along the direction perpendicular to the troughs, which in this case, is the X-axis. So in this configuration, we can expect the resultant average film stress in the X direction to be much smaller than the one in the Y direction, because of the stress relief from the substrate materials due to the edge effect. Therefore, this approach enables not just very effective stress relief, but also a highly non-equibiaxial stress state.

The resultant curvatures and stresses from all trough depths in the model series p200b15 are summarized and plotted in Fig. 9. Similar notations are used in this section as in the previous section. The simulated resultant substrate curvatures are normalized by κ^* where κ^* is substrate curvature in a uniform blanket film, as well as the substrate curvature before micromachined troughs are introduced into the substrate. Here, we use the dimensionless parameter "trough depth/trough separation" as the horizontal axis. The curvatures exhibit an interesting trend, which is discussed in the next section.
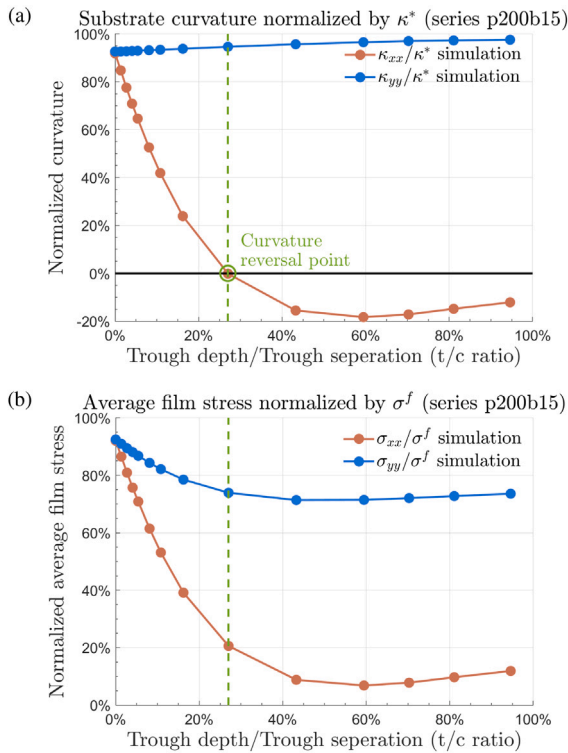
Fig. 9. Simulation results from the series of model with periodic trough pattern (p200b15): (a) Simulated resultant substrate curvatures normalized by κ^* (same definition as in Fig. 8); (b) Simulated resultant average film stresses normalized by $\sigma^{(f)}$(same definition as in Fig. 8). The green dash line marked by the circle indicates the location of curvature reversal in both figures.

Fig. 10. Illustration of the curvature reversal effect after machining of high t/c ratio troughs into the substrate along the direction perpendicular to the troughs.

Fig. 11. Simulated deformations in the Z-axis U_3 for thin-film/substrate system with periodic troughs and three varying trough depths. All figures are shown with a deformation scale factor of 1500 and units of μm. (a) When trough depth is small, the curvatures are both positive (bending downwards). (b) As trough depth increases to $t \approx 0.27c = 50\,\mu$m, the curvature in the direction perpendicular to trough (κ_{xx}) drops to zero. (c) When trough depth continues to increase, the curvature begins to reverse in the direction perpendicular to trough, indicated by an upward arrow.

4. Discussion

4.1. Curvature reversal & Poisson effect

As Fig. 9(a) shows, an interesting phenomena known as "curvature reversal" occurs in this series of simulations, at the point where $t/c \approx 0.27$. The curvature in the direction perpendicular to the trough (κ_{xx}) decreases rapidly as the trough depth increases. It drops below zero at the curvature reversal point and stays negative throughout with even deeper troughs. It does seem to come back up as the t/c ratio increases further, but this figure does not tell us if it will return back to zero at very high t/c ratio. (We have not simulated this extreme scenario as it becomes unrealistic to continue to increasing the trough depth t if we keep c the same, and it is also relatively unrealistic for actual applications. One way to do this is to simulate a series of very densely configured parallel troughs to keep the c small, so that we can continue to increase t without reaching the limit of the substrate thickness.) On the other hand, the curvature in the direction parallel to the trough (κ_{yy}) is slightly smaller than its value of $b\kappa^*/p$ at $t/c = 0$. This value, $b\kappa^*/p$, is a more suitable normalizing factor for curvature, since the "mean film thickness" in this case is $h_f b/p$. This value is also useful especially when comparing a number of different model configurations with different values of b, p. It seems that κ_{yy} asymptotically approaches κ^*, but again we cannot deduce that from this figure.

These observations can be explained by the Poisson effect, i.e., the coupling of strains in the in-plane orthogonal directions. The reversal of curvature perpendicular to the troughs is a consequence of the substrate's Poisson effect when highly anisotropic straining occurs [29], as in the case when the t/c ratio is large. Therefore, substrates with troughs of t/c ratios greater than 0.27 are forced to develop a reversed curvature in the X (κ_{xx}) direction induced by the higher stress in the Y (κ_{yy}) direction, due to the Poisson effect. Fig. 10 illustrates this
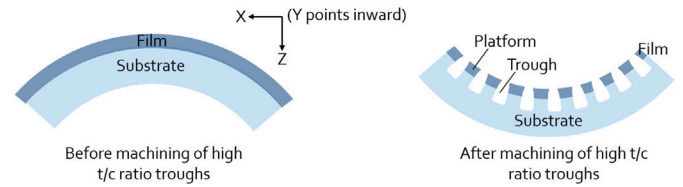
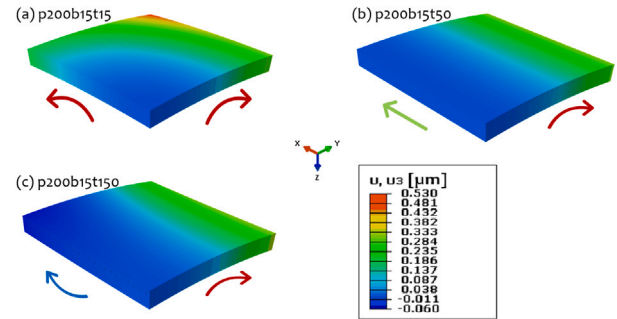curvature reversal effect after machining of high t/c ratio troughs into the substrate along the direction perpendicular to the troughs. Here, the platform refers to the section between neighboring troughs, especially as the t/c ratio becomes large or when trough depth t becomes comparable to trough separation c.

This curvature reversal effect can be seen in the transverse displacement in the simulated substrates described in this section. In Fig. 11, when trough depth is small, as in figure (a), the curvatures are both positive, indicated by red arrows bending downwards in both X and Y directions. As trough depth increases to $t \approx 0.27c = 50\,\mu$m, as in figure (b), the curvature in the direction perpendicular to the troughs (κ_{xx}) drops to zero, as shown by a green arrow along the X direction. When trough depth is very large, as in figure (c), the curvature reversal in the direction perpendicular to trough becomes obvious, which is shown in the figure by a blue arrow bending upwards along the X direction.

The curvature reversal can be exploited in figure correction application, to induce bending moments of different signs in the two biaxial directions. Yet, even though the curvatures present different signs, the stresses are all of the same sign, which can be seen in Fig. 9(b). The simulated resultant average film stresses are normalized by $\sigma^{(f)}$, where $\sigma^{(f)}$ is the intrinsic compressive stress of a uniform blanket film, as well as the film stress before micromachined troughs are formed in the substrate. In Fig. 9(b), both in-plane normal stresses in the direction perpendicular (σ_{xx}) and parallel (σ_{yy}) to the trough decrease gradually, but stress reversal does not happen. This means that the initial compressive stress in the blanket film cannot be fully relieved just by increasing the trough depth. In addition, the continuous range of ratios between the two in-plane stresses (σ_{xx}/σ_{yy}) renders a variety of choices for the selection of the combination of σ_{xx}, σ_{yy}, with a proper rotation of the trough direction [13], to generate stress fields that can correct for general figure errors in thin mirrors.

We have inspected a few other series of models, and the results are shown in Figs. 12 and 13. The ratio c/p is 85 % in the left model and 70 % in the right model, which determines the starting points of the normalized curvature and the normalized stress at $t/c = 0$. In all
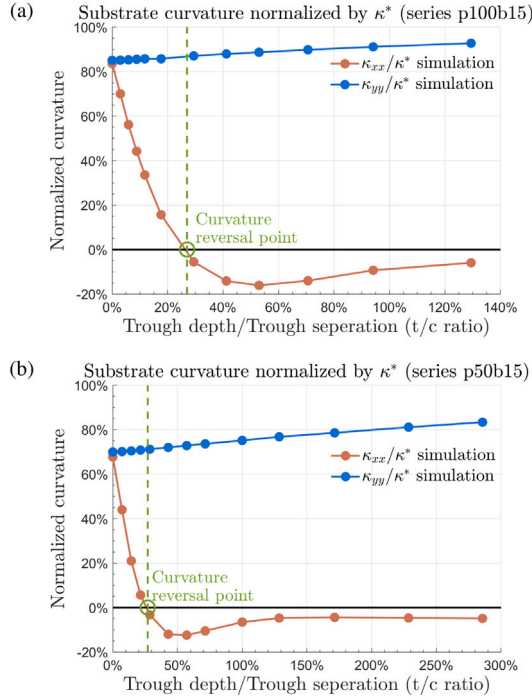
Fig. 12. Simulated resultant substrate curvatures normalized by κ^* for: (a) model series p100b15 (period 100 μm, trough width 15 μm) and (b) model series p50b15 (period 50 μm, trough width 15 μm). The green dash lines indicate the location of curvature reversal in both figures, same as Fig. 9.
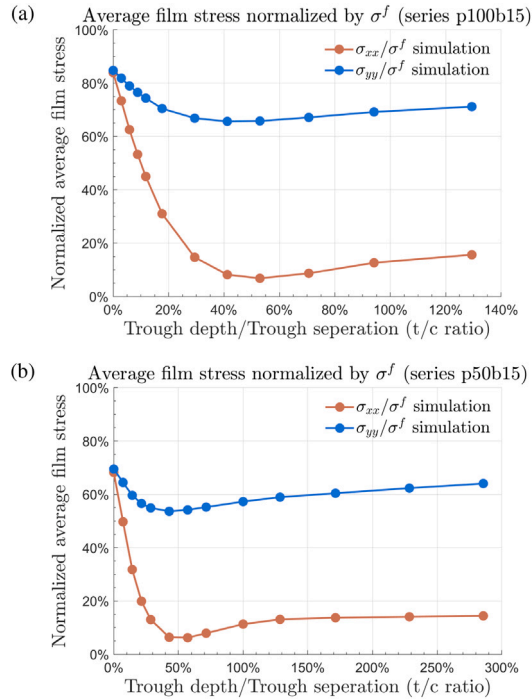

Fig. 13. Simulated resultant average film stress normalized by $\sigma^{(f)}$ for: (a) model series p100b15 (period 100 μm, trough width 15 μm) and (b) model series p50b15 (period 50 μm, trough width 15 μm).

three cases (including p200b15 series), we observed that the curvature reversal happens at about $t/c \approx 0.27$ empirically, for they have the same film thickness $h_f = 0.5$ μm. We have simulated other film thicknesses and the curvature reversal point changed. Additionally, in all three
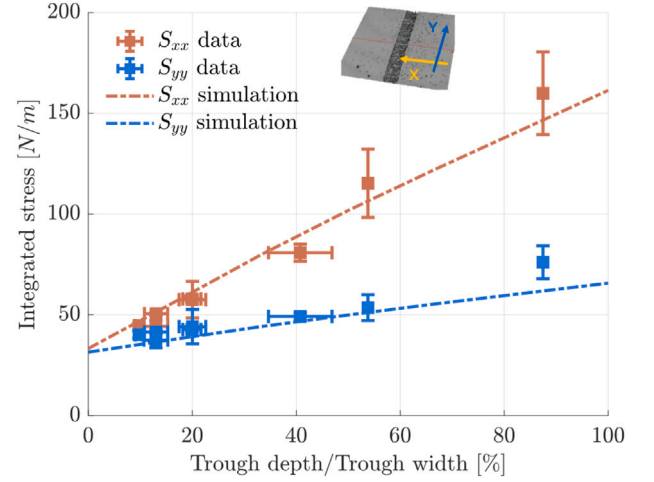

Fig. 14. Difference of the integrated stress fields from experiments (square with error bars) and simulations (dash line) with periodic trough pattern are compared for the same 200 μm trough period, which are the scattered data with error bars originally shown in Fig. 3. The inset is taken from Fig. 2(b) and shows one section of the micromachined trough and how the two axial directions X and Y are defined.

cases, the two in-plane normal stresses in the direction perpendicular (σ_{xx}) and parallel (σ_{yy}) to the trough both decrease first, followed by a slow increase. Like the case with the curvatures, we speculate the location of this turning point also depends on dimensionless parameters that include the film thickness, such as h_f/b or h_f/p.

4.2. Comparison with experiments

The simulation needs to be compared with the experimental results to verify its credibility and build consistency with physical systems. To do this, we simulate the same structure as realized in the experiment, and plot their results against each other in Fig. 14. The fields that are compared are changes of the integrated stresses in the two axial directions in the trough model. The period in the experiments and simulations is 200 μm. The experimental observations include 8 micromachined samples with various trough depths and widths. The original figure of the change of the integrated stress field for six of the plotted samples is shown in Fig. 3. In addition, the horizontal error bar indicates the variance in the measurements of the feature size (trough depths and widths) in one sample, and the vertical error bar shows the variance in the calculated integrated stress field over the same sample. The inset shows one section of the micromachined trough and how the two axial directions X and Y are defined.

The simulations are part of the Abaqus model series p200b15, which simulates the thin-film/substrate system with periodic troughs and varying trough depths. The original results shown in Fig. 9(b) are the resultant average film stresses. In Fig. 3, we show the differences of the stress fields, i.e., the differences between the resultant average film stress and the original blanket film stress. The continuous curves are interpolations of individual simulation points. Note that the blanket film stress used in the simulations is set at 420 MPa to match the experiments.

Fig. 14 shows that the simulations match with the experiments quite well at smaller aspect ratios (less than 100 %). The differences between each pair of the data are calculated, and the maximum difference is less than 18 %. Therefore, we have achieved a reasonably good agreement (> 82 %) between simulations and experimental observations.

4.3. "Equivalent trough width" assumption

As we have seen earlier in Fig. 3, at small trough depths the laser-induced stress relief effect forms a quasi-linear relationship with the
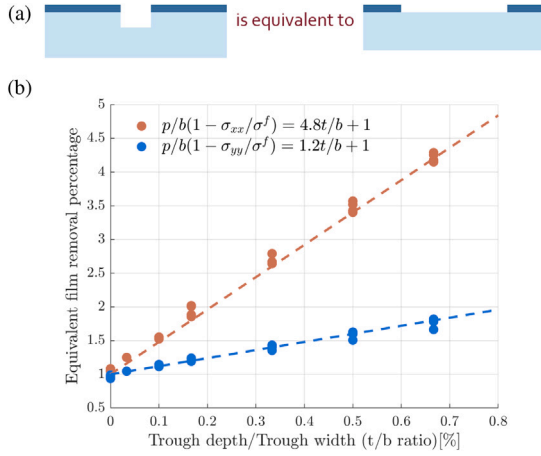
(a)

is equivalent to

(b)

Fig. 15. "Equivalent trough width" assumption for characterizing the stress relief effect: (a) Increasing the trough depth t is assumed to be equivalent to extending the trough width b by a correction factor of M on each side of the trough. (b) The change of the integrated stress field is proportional to the equivalent film removal percentage, i.e., $\frac{p}{b}\left(1 - \frac{\sigma_\alpha}{\sigma^{(f)}}\right) = 2M_\alpha \frac{t}{b} + 1$. The correction factor is 2.4 for σ_{xx}, and 0.6 for σ_{yy}.

ratio of the trough depth divided by its width. Now we explore this observation in further detail. Since the simulations match well with the experiments at small trough ratio, we use the data from several series of the FEM simulations in the following analysis.

The purpose of this section is to explain the observed quasi-linear relationship between the stress relief effect from the micromachined features and the dimensionless trough ratio. As a starting point, we assume the change of the integrated stress field is proportional to the removal percentage of the stressed film. Since removing substrate material adjacent to the film leads to further stress relief, this can be thought of as removing not substrate material but additional film material, as shown in Fig. 15(a). Therefore, increasing the trough depth t is equivalent to extending the trough width b by a correction factor of M on each side of the trough, so the equivalent film removal percentage is $(2Mt + b)/p$. Following this assumption, the change of the integrated stress field is then proportional to the equivalent film removal percentage, i.e., $1 - \frac{\sigma_\alpha}{\sigma^{(f)}} = \frac{2M_\alpha t + b}{p}$. This relationship can be rewritten as $\frac{p}{b}\left(1 - \frac{\sigma_\alpha}{\sigma^{(f)}}\right) = 2M_\alpha \frac{t}{b} + 1$, where the subscript α represents either xx or yy.

Then we fit the simulated stress relief ratio $\left(1 - \frac{\sigma_\alpha}{\sigma^{(f)}}\right)$ as a function of the trough ratio t/b and solve for M_α. The results are shown in Fig. 15(b), where the correction factors are $M_{xx} = 2.4$ and $M_{yy} = 0.6$. The results can be written as:

$$\frac{p}{b}\left(1 - \frac{\sigma_{xx}}{\sigma^{(f)}}\right) \approx 4.8\frac{t}{b} + 1, \qquad \frac{p}{b}\left(1 - \frac{\sigma_{yy}}{\sigma^{(f)}}\right) \approx 1.2\frac{t}{b} + 1. \qquad (2)$$

Plugging this relationship back into Stoney's equations, we obtain the dependence of the normalized curvatures on the trough ratio as:

$$\begin{aligned}\frac{p}{b}\frac{\kappa_{xx}}{\kappa^*} &\propto -\frac{2(M_1 - \nu_s M_2)}{1 - \nu_s^2}\frac{t}{b} \approx -4.7\frac{t}{b}, \\ \frac{p}{b}\frac{\kappa_{yy}}{\kappa^*} &\propto -\frac{2(M_2 - \nu_s M_1)}{1 - \nu_s^2}\frac{t}{b} \approx -0.9\frac{t}{b},\end{aligned} \qquad (3)$$

where the subscript s denotes the substrate, whose in-plane Poisson ratio is 0.064 for a (100) Si wafer.

This analysis approach could also cover other stress change effects beyond stressed film material removal, such as potential local stress changes in the Si substrate. In addition, this analysis is not just useful in choosing proper micromachining parameters, but it also serves as a comparison to the aforementioned estimates in Section 3.1. In the case where the trough structure exists only in the film, Freund and Suresh [23] provided simple estimates for the principal curvatures κ_{xx}, κ_{yy}

of a substrate as a function of the Poisson ratios of the film ν_f and substrate ν_s, as well as a dimensionless length $\frac{l}{b}$, where l is a parameter with physical dimension of length proportional to h_f. Using further simplifications and taking the numerical values of the Poisson ratios for SiO$_2$ as the film and Si as the substrate, we obtain the formulae for the normalized curvatures as

$$\frac{p}{b}\frac{\kappa_{xx}}{\kappa^*} \propto -4.2\frac{h_f}{b}, \qquad \frac{p}{b}\frac{\kappa_{yy}}{\kappa^*} \propto -0.5\frac{h_f}{b}. \qquad (4)$$

These formulae take similar formats as the approximations that we obtained earlier, except for the use of h_f instead of t since here $h_f = t$. The magnitude of the coefficients are comparable, because the nature of the problems are similar at shallow troughs. But the coefficients in both curvatures are larger ($4.7 > 4.2$, $0.9 > 0.5$), which indicates the additional stress relief effect that comes from the edge effect when machining into the substrates. It is also worth noticing that both the approximations and estimates only apply to the case of shallow troughs.

4.4. Comparison between "periodic film/substrate model" and "periodic film model"

Shen et al. [29] have studied the evolution of stresses and changes in curvatures due to the patterning of silicon oxide lines, obtained by etching lines into the oxide film but not into the silicon substrate. Yet, there are a lot of similarities between these two problems, so we can compare the trends of the changes of stresses and curvatures for both models. A difference is that the predicted average stresses in the lines of oxide films normalized by the corresponding film stress, in their case, decreases asymptotically as a function of t/c for various ratios of p/c.[2] Also, they found the curvature reversal point to be at $t/c \approx 0.4$. Further, they have theorized the asymptotic value of the curvature in the case of $t/c \to \infty$ to be $\kappa_{yy}/\kappa_{xx} \to -\nu_{Si}$. All of these, however, do not agree with our observations for the "periodic film/trough model" that is studied in this paper. We have seen the value of the resultant average stresses to decrease then increase with the increasing t/c ratio. We have found for at least three models that the curvature reversal point is located at around $t/c \approx 0.27$. And the asymptotic value, even if exists in our model, does not appear to be $-\nu_{Si}$ (negative Poisson ratio of silicon substrate).

The main cause for the difference is, of course, the different trough structure. But we want to compare with the "periodic film model" because the only difference in the structure is that for their model $(t + h_f)/h_f = 1$, but for our "periodic film/trough model" it is not a constant number and $(t + h_f)/h_f \geq 1$. So, this dimensionless ratio t/h_f, or any other dimensionless ratio involving film thickness h_f, must be included in the asymptotic analysis. Therefore, for their model, two dimensionless parameters $t/c, p/c$ are enough; while in our model, a third parameter must be included. Hence, we speculate that the location of the curvature reversal point, the turning point and asymptotic value of the curvatures and stresses are all functions of the film thickness ratio t/h_f, along with other ratios $t/c, p/c$. Further, as there is no analytical solution to the aforementioned points, only numerical values are available that could be obtained from FEM analysis, and we here provided one of them for a specific film thickness.

5. Conclusion

We have developed a stressed film figuring method for the shape correction of thin silicon mirrors using femtosecond laser micromachining through the removal of selective stressed film regions and adjacent substrate regions. This method has been demonstrated on flat silicon mirrors with the patterning of a stressed film of thermal oxide.

---

[2] The authors originally used w as the film width, which is the same as c in our model. For better comparison between the models, we have used c instead of w here.

In this paper, we have presented both experimental and numerical results for the laser-induced stresses and curvature changes of thin mirrors with different micromachined features. Two types of periodic patterns have been studied, each with varying feature geometries, to represent the influence of various micromachining parameters. Periodic hole patterns create equibiaxial stress, and periodic trough patterns lead to non-equibiaxial stress. Specifically, our 3D FEM model enables the prediction of substrate deformation in directions parallel and perpendicular to the patterned troughs. In general, the hole pattern model leaves higher residual stress, indicating a lower amount of stress relief. The resultant substrate stress is mostly concentrated near the film/substrate interface, along the wall of the ablated geometries. This edge effect contributes to the additional stress relief when machining into the substrate. In addition, the laser affected regions increase in scale as the troughs or holes become deeper. It is also shown that implementing high aspect ratio troughs micromachined into the substrate can induce curvature reversal in the direction perpendicular to the troughs. Numerical results from the finite element simulation are compared to experimental observations for several different geometrical combinations of the depth, width and spacing of the patterned troughs, and good agreement has been achieved.

The findings in this paper can become handy in determining the optimal parameters for the stressed film patterns used in the stress compensation and figure correction steps for thin optics. The method descried here may enable more precise, scalable, and cheaper production of space optics, allowing larger telescopes that can be sent into space at lower cost.

CRediT authorship contribution statement

Heng E. Zuo: Conceptualization, Methodology, Data curation, Formal analysis, Investigation, Software, Validation, Visualization, Writing – original draft. **Ralf K. Heilmann:** Conceptualization, Methodology, Validation, Supervision, Writing – review & editing. **Mark L. Schattenburg:** Conceptualization, Methodology, Funding acquisition, Project administration, Resources, Validation, Supervision, Writing – review & editing.

Declaration of competing interest

The authors declare that they have no known competing financial interests or personal relationships that could have appeared to influence the work reported in this paper.

Data availability

Data will be made available on request.

Acknowledgments

References

[1] K. Patterson, S. Pellegrino, Ultralightweight deformable mirrors, Appl. Opt. 52 (22) (2013) 5327–5341.

[2] J.A. Gaskin, D. Swartz, A.A. Vikhlinin, F. Özel, K.E. Gelmis, J.W. Arenberg, S.R. Bandler, M.W. Bautz, M.M. Civitani, A. Dominguez, et al., Lynx X-ray observatory: an overview, J. Astron. Telesc. Instrum. Syst. 5 (2) (2019) 021001.

[3] B.D. Chalifoux, R.K. Heilmann, H.L. Marshall, M.L. Schattenburg, Optical design of diffraction-limited x-ray telescopes, Appl. Opt. 59 (16) (2020) 4901–4914.

[4] Y. Sun, S. Izumi, S. Sakai, K. Yagi, H. Nagasawa, Saddle-shape warpage of thick 3C-SiC wafer: Effect of nonuniform intrinsic stress and stacking faults, Phys. Status Solidi (B) 249 (3) (2012) 555–559.

[5] A. Mallik, R. Stout, J. Ackaert, Finite-element simulation of different kinds of wafer warpages: spherical, cylindrical, and saddle, IEEE Trans. Compon. Packag. Manuf. Technol. 4 (2) (2014) 240–247.

[6] D. Shi, Z. Xia, M. Hu, G. Mei, Z. Huo, A novel solution to improve saddle-shape warpage in 3D NAND flash memory, Semicond. Sci. Technol. 35 (4) (2020) 045031.

[7] J.P. Rolland, M.A. Davies, T.J. Suleski, C. Evans, A. Bauer, J.C. Lambropoulos, K. Falaggis, Freeform optics for imaging, Optica 8 (2) (2021) 161–176.

[8] S. Trolier-McKinstry, P. Muralt, Thin film piezoelectrics for MEMS, J. Electroceram. 12 (1) (2004) 7–17.

[9] C.T. DeRoo, R. Allured, V. Cotroneo, E.N. Hertz, V. Marquez, P.B. Reid, E.D. Schwartz Sr, A.A. Vikhlinin, S. Trolier-McKinstry, J. Walker, et al., Deterministic figure correction of piezoelectrically adjustable slumped glass optics, J. Astron. Telesc. Instrum. Syst. 4 (1) (2018) 019004.

[10] B. Chalifoux, Y. Yao, H.E. Zuo, R.K. Heilmann, M.L. Schattenburg, Compensating film stress in silicon substrates for the Lynx X-ray telescope mission concept using ion implantation, in: Space Telescopes and Instrumentation 2018: Ultraviolet To Gamma Ray, Vol. 10699, International Society for Optics and Photonics, 2018, 1069959.

[11] B.D. Chalifoux, Y. Yao, K.B. Woller, R.K. Heilmann, M.L. Schattenburg, Compensating film stress in thin silicon substrates using ion implantation, Opt. Express 27 (8) (2019) 11182–11195.

[12] Y. Yao, B.D. Chalifoux, R.K. Heilmann, M.L. Schattenburg, Thermal oxide patterning method for compensating coating stress in silicon substrates, Opt. Express 27 (2) (2019) 1010–1024.

[13] Y. Yao, B. Chalifoux, R.K. Heilmann, M.L. Schattenburg, Stress tensor mesostructures for deterministic figuring of thin substrates, Optica 9 (4) (2022) 438–444.

[14] B.D. Chalifoux, R.K. Heilmann, M.L. Schattenburg, Correcting flat mirrors with surface stress: analytical stress fields, J. Opt. Soc. Amer. A 35 (10) (2018) 1705–1716.

[15] H.E. Zuo, B.D. Chalifoux, R.K. Heilmann, S.-H. Nam, K.-H. Hong, M.L. Schattenburg, Demonstration of femtosecond laser micromachining for figure correction of thin silicon optics for x-ray telescopes, in: Optics for EUV, X-Ray, and Gamma-Ray Astronomy IX, Vol. 11119, International Society for Optics and Photonics, 2019, 111191A.

[16] H. Zuo, R. Heilmann, M. Schattenburg, Femtosecond laser micromachining for stress-based figure correction of thin mirrors, Optica 9 (10) (2022) 1163–1175.

[17] C.M. Beckmann, L.J. Richter, J. Ihlemann, Freeform shaping of fused silica substrates via viscous deformation induced by a laser patterned, stressed film, Opt. Express 30 (5) (2022) 6726–6737.

[18] B.D. Chalifoux, K.A. Laverty, I.J. Arnold, Ultrafast laser stress figuring for accurate deformation of thin mirrors, Opt. Express 30 (11) (2022) 17767–17780.

[19] E. Kobeda, E. Irene, Intrinsic SiO_2 film stress measurements on thermally oxidized Si, J. Vac. Sci. Technol. 5 (1) (1987) 15–19.

[20] J. Fitch, C. Bjorkman, G. Lucovsky, F. Pollak, X. Yin, Intrinsic stress and stress gradients at the SiO_2/Si interface in structures prepared by thermal oxidation of Si and subjected to rapid thermal annealing, J. Vac. Sci. Technol. 7 (4) (1989) 775–781.

[21] H.E. Zuo, Ultrafast laser micromachining for correction of thin optics for next generation X-ray space telescopes, (Ph.D. thesis), Massachusetts Institute of Technology, 2021.

[22] G.G. Stoney, The tension of metallic films deposited by electrolysis, Proc. R. Soc. Lond. Ser. A 82 (553) (1909) 172–175.

[23] L.B. Freund, S. Suresh, Thin Film Materials: Stress, Defect Formation and Surface Evolution, Cambridge University Press, 2004.

[24] M.J. Smith, Y.-T. Lin, M.-J. Sher, M.T. Winkler, E. Mazur, S. Gradečak, Pressure-induced phase transformations during femtosecond-laser doping of silicon, J. Appl. Phys. 110 (5) (2011) 053524.

[25] A. Ionin, S. Kudryashov, A. Levchenko, L. Nguyen, I. Saraeva, A. Rudenko, E. Ageev, D. Potorochin, V. Veiko, E. Borisov, et al., Correlated topographic and structural modification on si surface during multi-shot femtosecond laser exposures: Si nanopolymorphs as potential local structural nanomarkers, Appl. Surf. Sci. 416 (2017) 988–995.

[26] J. Beuth Jr., Cracking of thin bonded films in residual tension, Int. J. Solids Struct. 29 (13) (1992) 1657–1675.

[27] Z.C. Xia, J.W. Hutchinson, Crack patterns in thin films, J. Mech. Phys. Solids 48 (6–7) (2000) 1107–1131.

[28] J. Dundurs, Discussion:"Edge-bonded dissimilar orthogonal elastic wedges under normal and shear loading", 1969, Bogy, DB, 1968, ASME J. Appl. Mech., 35, pp. 460–466.

[29] Y.-L. Shen, S. Suresh, I. Blech, Stresses, curvatures, and shape changes arising from patterned lines on silicon wafers, J. Appl. Phys. 80 (3) (1996) 1388–1398.

[30] Y. Yao, B.D. Chalifoux, R.K. Heilmann, K.-W. Chan, H. Mori, T. Okajima, W.W. Zhang, M.L. Schattenburg, Progress of coating stress compensation of silicon mirrors for Lynx x-ray telescope mission concept using thermal oxide patterning method, J. Astron. Telesc. Instrum. Syst. 5 (2) (2019) 021011.

[31] M.A. Hopcroft, W.D. Nix, T.W. Kenny, What is the Young's modulus of silicon? J. Microelectromech. Syst. 19 (2) (2010) 229–238.

[32] AZO Materials, Silica - silicon dioxide (SiO_2), 2011, https://www.azom.com/article.aspx?ArticleID=1114.